Available online at www.sciencedirect.com
SCIENCE DIRECT
International Journal of Heat and Fluid Flow 26 (2005) 905–913
International Journal of HEAT AND FLUID FLOW
www.elsevier.com/locate/ijhff

Thermal-field structure of a non-premixed turbulent flame formed in a strong pressure-gradient flow

M. Tagawa *, M. Fukatsu, Y. Nabata, Y. Ohta

Department of Mechanical Engineering, Nagoya Institute of Technology, Gokiso-cho, Showa-ku, Nagoya 466-8555, Japan

Available online 9 November 2005

Abstract

Statistical characteristics of a non-premixed turbulent flame formed in a curved-rectangular duct and spatio-temporal structures of the thermal field were investigated experimentally. The flame was much affected by a strong pressure gradient in the radial direction of the duct curvature, which caused strong gradient diffusion in turbulent heat transfer on the inner-wall side of the flame and, in contrast, counter-gradient heat transfer on the outer-wall side. Two-point correlation measurement of temperature fields revealed that, in the strong gradient diffusion region, a spatial thermal pattern generated by turbulent mixing of high- and low-temperature fluid parcels was advected downstream with little diffusion. In contrast, the pattern was attenuated and diffused rapidly in the counter-gradient diffusion region. These results accurately correspond to the generation mechanism of the counter-gradient heat transport so far observed in stably stratified turbulent flows.

Keywords: Combustion; Turbulence; Heat transfer; Counter-gradient diffusion

1. Introduction

Non-premixed turbulent flames are widely used for combustors of boilers, gas turbines, industrial furnaces, etc., and the flow passages or walls of the combustors are often curved. In our previous study (Tagawa et al., 2002), we reported that a "counter-gradient diffusion" phenomenon of heat transfer emerged when a strong pressure gradient was externally imposed on a non-premixed turbulent flame using a curved duct. The counter-gradient diffusion is regarded as an unusual phenomenon in which "turbulence" will diminish momentum and/or scalar transport. For example, in a field having a counter-gradient heat transfer, we may see turbulent heat transfer occur against the mean-temperature gradient, a phenomenon that is, of course, counter to our intuition.

Recently, the direct numerical simulation (DNS) of premixed turbulent flames (Rutland and Cant, 1994; Zhang and Rutland, 1995; Nishiki et al., 2002) provided a quantitative appraisal of each term of the transport equation for a turbulent scalar flux, and made clear the significance of the pressure-related terms. Furthermore, based on the results of both DNS (Veynante and Poinsot, 1997) and experimental (Kalt et al., 2002) investigations, the influence of an externally imposed mean pressure gradient on the counter-gradient diffusion of a scalar (reaction progress variable) has been discussed. These studies have shown that the counter-gradient diffusion of premixed turbulent flames can well be characterized by a Bray number (Veynante et al., 1997; Bray, 1995) or a modified version of the number (Kalt et al., 2002) [the Bray number N_B is defined as $N_B = \tau u_L/2\alpha u_{rms}$ (τ: heat release factor, $T_p/T_r - 1$, where the subscripts p and r represent products and reactants; u_L: laminar burning velocity; α: specified function of the ratio of integral length scale of turbulence to laminar flame thickness) and is a criterion indicating the occurrence of gradient or counter-gradient diffusion in atmospheric premixed turbulent flames].

* Corresponding author. Tel./fax: +81 52 735 5343.
E-mail address: m.tagawa@nitech.ac.jp (M. Tagawa).

0142-727X/$ - see front matter © 2005 Elsevier Inc. All rights reserved.
doi:10.1016/j.ijheatfluidflow.2005.10.006

Nomenclature

Q*i*	*i*th quadrant in (v', t')-plane
r, θ, z	cylindrical coordinate for curved duct (Fig. 1)
T, t	temperature and its fluctuation
U, V	velocity components in θ- and r-directions
u, v	velocity fluctuation components in θ- and r-directions
y	distance from inner-wall surface ($= r - r_i$; r_i: radius of curvature of inner wall)

Symbols

$(\ )_{rms}$	root-mean-square value
$\overline{(\ )}$	Reynolds average (conventional time average)
$\widetilde{(\ )}$	Favre average (density-weighted time average)
$(\ )'$	fluctuation from Reynolds average
$(\ )''$	fluctuation from Favre average
$\langle\ \rangle$	statistical (Reynolds/Favre) average

As for the counter-gradient diffusion of non-premixed turbulent flames, experimental data have long been accumulated, as cited in our previous paper (Tagawa et al., 2002). At the present stage, however, there are few studies that provide systematic information on the characteristics of counter-gradient diffusion mainly because of the complex nature peculiar to the non-premixed flame. Theoretical approaches that can reveal the universal nature of counter-gradient diffusion are also limited (Jones, 1994). Recently, detailed features of the counter-gradient diffusion of non-premixed flames have gradually been revealed from the DNS of a flame formed in a supersonic mixing layer (Luo and Bray, 1998) and from a jet flame experiment (Caldeira-Pires and Heitor, 2001).

As seen in these studies, when we focus attention on the behaviors of high-temperature fluid parcels (low-density burnt gas), it would be natural to expect the existence of essential physical processes common to the counter-gradient diffusion phenomena of both premixed and non-premixed turbulent flames. For example, since a heat release factor (Libby and Bray, 1981)—a principal constituent of the Bray number—is in direct proportion to the burnt gas temperature, we expect that the onset mechanism of the counter-gradient diffusion of a non-premixed turbulent flame will be closely related to the behavior of the high-temperature fluid parcels of the flame.

The objective of the present study is to reveal the underlying mechanism of the onset of a counter-gradient heat transfer, and to understand the essential features of the transport phenomena in non-premixed turbulent flames. In practice, such information will be useful in establishing effective strategies for manipulating the geometrical aspects of turbulent flames, e.g., shape, size, length and position, and for controlling heat transfer to the combustor walls and reducing toxic combustion emissions.

Specifically, we investigate statistical behaviors of the important turbulence quantities of velocity and temperature with the aid of various useful tools for analyzing the structure of turbulent phenomena. Furthermore, we apply a two-point correlation measurement technique to the analysis of the temperature field of the non-premixed flame, and investigate the effects of the pressure gradient on spatio-temporal structures of the turbulent thermal field, which are closely related to the onset mechanism of the counter-gradient diffusion in heat transport. Such approaches will reveal the internal turbulence structure of a non-premixed turbulent flame and identify the elementary heat transfer processes under an externally imposed mean pressure gradient.

2. Experimental apparatus and procedure

Fig. 1 shows the combustor and coordinate system used. The flow passage of the combustor is a 180° curved duct (U-bend) with one end connected to a wind tunnel. The cross-sectional area of the curved-rectangular duct was 50×80 mm^2. The airflow at the inlet ($\theta = 0°$) was uniform, and its average velocity was 7.7 m/s. The free stream turbulence at the combustor inlet was 7% in relative intensity, which was generated by a perforated plate (hole size ϕ 5 mm, pitch 7 mm) set 100 mm upstream from the inlet. The fuel used was propane and was supplied at a flow rate of 3.0 L/min from the fuel exit (5×50 mm^2) located at the center of the inlet. The velocity components in the r- and θ-directions (Fig. 1) are denoted by V and U, respectively. The principal test section of the present experiment is located 60° from the combustor inlet and in the symmetry plane of the duct ($z = 0$ mm).

The combustion field was measured using a simultaneous velocity and temperature measurement technique based on the LDV (laser Doppler velocimetry) and a digitally compensated fine-wire thermocouple probe (Hardalupas et al.,

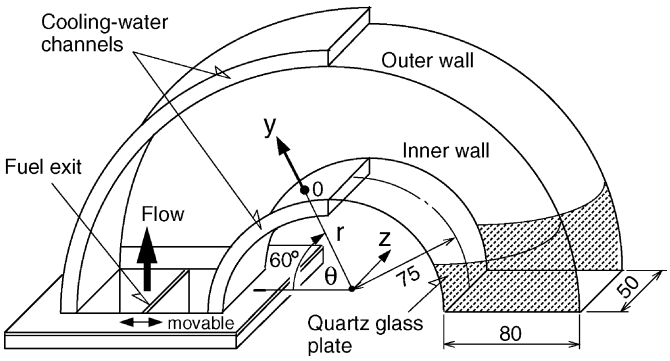

Fig. 1. Combustion chamber and coordinate system.

1996). The details of the technique were described in our previous papers (Tagawa and Ohta, 1997; Tagawa et al., 2001). A type-R thermocouple 40 μm in diameter was used, and its response was compensated with the time-constant value of 16 ms (Tagawa et al., 2002). In the LDV measurement, alumina particles (1 μm in nominal diameter) were used to seed the flow field, and the number density of the seeding particles was kept sparse. The possible non-uniformity in the particle number-density distribution had little effect on the measurement (see Appendix A). In the two-point correlation measurement of the temperature field, we used two fine-wire thermocouple probes, which were arranged so as to minimize fluid-dynamical interference between them. The test section ranged from $\theta = 45°$ to 75° in the central ($z = 0$ mm) plane. Turbulence quantities were obtained from 1024 samples of velocity and temperature data, and the statistical analysis and the two-point correlation measurement were executed using 32,768 and 10,000 samples, respectively, to reduce uncertainties in the statistical results.

3. Results and discussion

3.1. Thermal-field turbulence quantities

Fig. 2 shows the schlieren image of the flame formed in the curved duct. The flame is formed concentrically with the inner and outer walls of the duct and is nearly planar in the z-direction. As seen from Fig. 2, fluid motions at the inner-wall (low-pressure) side are very active, whereas they are inactive at the outer-wall (high-pressure) side, and there exists a clear boundary. Since a strong positive pressure gradient $d\overline{p}/dr \simeq 6 \times 10^2$ Pa/m is imposed on the flow field, the low-density (high-temperature) burnt gas can be considered to be placed on the high-density (low-temperature) gas at the outer-wall side of the flame, and a state similar to a stably stratified flow is realized there. On the inner-wall (low-pressure) side, however, the high-density gas is placed on the low-density gas as in the case of an unstably stratified flow. Consequently, two contrasting turbulent fields in terms of flow stability coexist in the combustion field formed in the curved duct.

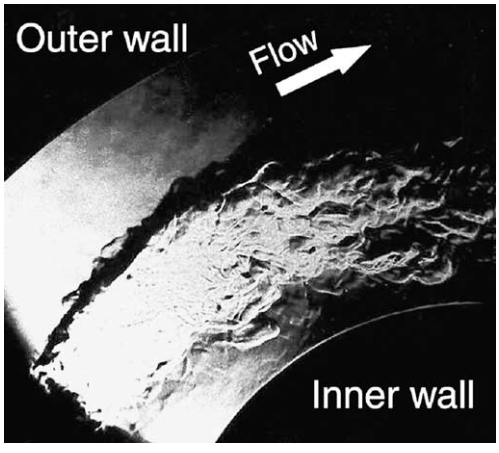

Fig. 2. Flame formed in duct center (schlieren image) (Tagawa et al., 2002).

Since the turbulent combustion is accompanied by large density fluctuations, the Favre (density-weighted) averaging is often used to eliminate apparently most of the effects of density fluctuation on the transport equations of turbulence quantities. Fig. 3 shows the y-direction distributions of the Reynolds-averaged turbulence quantities measured at $\theta = 60°$, $\sqrt{\overline{v'^2}}$, $\overline{T}$, $\sqrt{\overline{t'^2}}$ and $\overline{v't'}$, in comparison with the Favre-averaged counterparts [error bars in Fig. 3 show their variations corresponding to substantial changes in the thermocouple time-constant value (16 ± 4 ms)]. As seen from Fig. 3, the Favre-averaged values are smaller than the Reynolds-averaged ones by 20–30% around $y = 40$ mm, where the intensity of the temperature fluctuations is largest. However, we can see little qualitative difference between them. Hence, the results obtained may be universal irrespective of which method of statistical averaging is employed.

From Fig. 3, we find that the mean-temperature distribution of the flame exhibits a gradual ascent on the inner-wall side and a steep descent on the outer-wall side around $y = 50$ mm. As pointed out previously (Tagawa et al., 2002), turbulence mixing in the inner-wall region is very active, leading to a marked increase in v_{rms} and to a gently sloping mean-temperature distribution. In contrast,

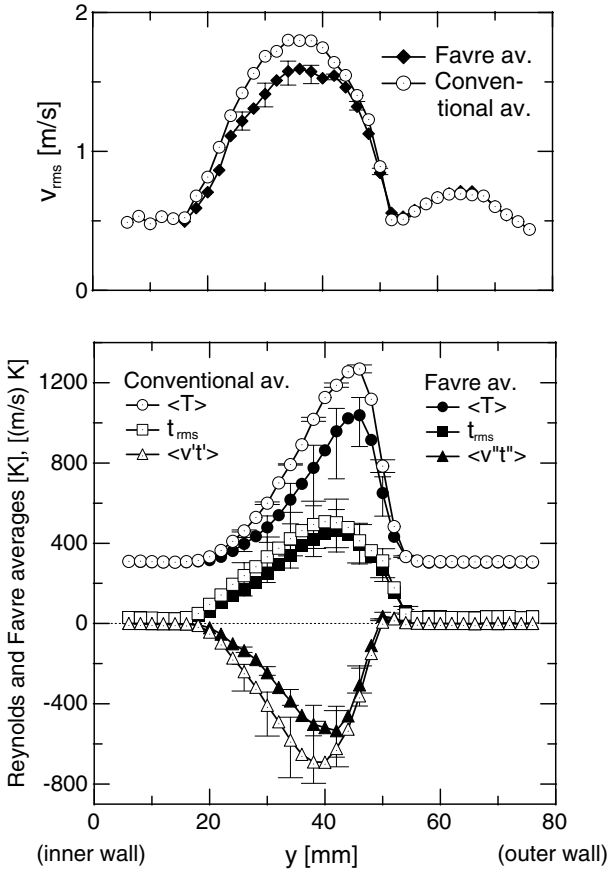

Fig. 3. Distributions of turbulence quantities ($\theta = 60°$) (Tagawa et al., 2002).

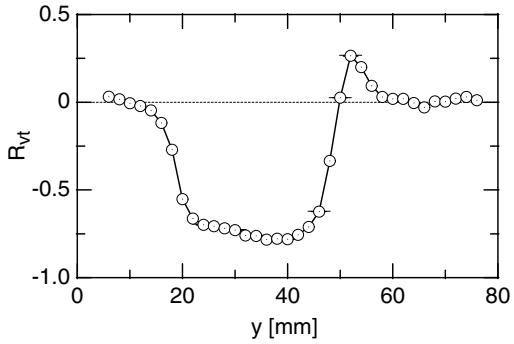

Fig. 4. Cross-correlation coefficient between v' and t' (Tagawa et al., 2002).

turbulence mixing in the outer-wall region is weak, and the thermal field is in a peculiar state as if the high-temperature region were shielded from the outer low-temperature region, though the flow is turbulent. Usually, a turbulent heat-flux $\overline{v't'}$ behaves in the gradient-type diffusion manner expressed as $\overline{v't'} \propto -\partial\overline{T}/\partial y$. As seen from Fig. 3, $\overline{v't'}$ is negative with $\partial\overline{T}/\partial y$ positive in the $y < 40$ mm region. This state represents gradient-type diffusion, but it is far more remarkable than usual, since the cross-correlation coefficient between v' and t' indicates quite a large negative value of -0.8 in this region as evident from Fig. 4 (Tagawa et al., 2002). The coefficient is rarely below -0.5 in ordinary turbulent thermal fields. In the outer-wall region of $y > 46$ mm, however, $\overline{v't'}$ remains negative when $\partial\overline{T}/\partial y$ turns negative. This indicates the onset of the counter-gradient diffusion in heat transport. The counter-gradient diffusion shown in Fig. 3 is relatively weak, since $\overline{v't'}$ remains slightly negative or nearly zero around $y = 50$ mm where $\partial\overline{T}/\partial y$ becomes steepest.

3.2. Statistical characteristics of velocity and temperature fluctuations

The turbulence statistics of the flame are investigated at the following three y positions: $y = 34$ mm where the strong gradient-diffusion heat transfer was observed; $y = 44$ mm at which the mean-temperature $\overline{T}$ peaked; and $y = 50$ mm where the counter-gradient heat transfer emerged. Figs. 5 and 6 show the probability density functions (pdfs) of velocity V [m/s] and temperature T [K], respectively, with the corresponding signal traces of T shown in Fig. 7.

As seen from Fig. 5, the pdf distributions of V are distinctly different between $y = 34$ mm and $y = 50$ mm. On the inner-wall side of the flame ($y = 34$ mm), the pdf is skewed in the negative direction because of the existence of large-amplitude fluid motions approaching the inner wall ($V < 0$). In contrast, on the outer-wall side of the flame ($y = 50$ mm), such motions are strongly suppressed, and this makes the pdf considerably sharp.

However, as seen from Fig. 6, the pdf of T at $y = 34$ mm resembles that at $y = 50$ mm, although they peak at different temperatures. Both are highly skewed to the high-temperature region. Despite such similarity in these two pdfs, the signal traces shown in Fig. 7 indicate a rather different picture. On the inner-wall side ($y = 34$ mm), the signal trace exhibits a very intermittent nature, that is, it rises steeply from the baseline temperature ($\simeq$300 K) of the airflow supplied to the combustor. This feature results from the very active high-temperature fluid parcels moving toward the inner wall as observed in the schlieren photograph (Fig. 2). The signal trace obtained at $y = 50$ mm, on the other hand, has no such distinct baseline and indicates little intermittency. Furthermore, the fluctuation appears to be less active than that at $y = 34$ mm. In the inner-wall region involving a strong gradient-diffusion heat transfer, the correlation between v' and t' was extremely high ($R_{vt} \simeq -0.8$) as seen from Fig. 4. Thus, such characteristics of the V and T pdfs can be ascribed to the high correlation between v' and t', and are reflected in the intermittent and active temperature signal trace seen in Fig. 7. However, in the outer-wall region where a weak

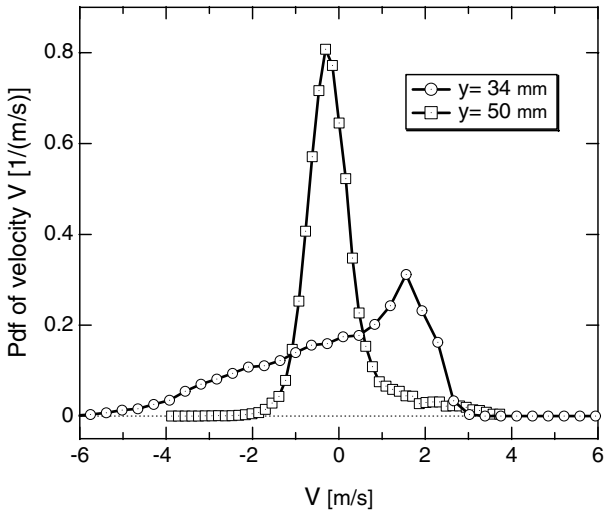

Fig. 5. Probability density functions of V.

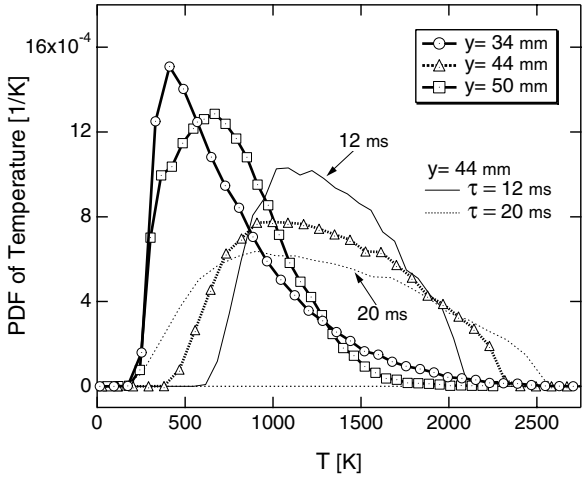

Fig. 6. Probability density function of T.

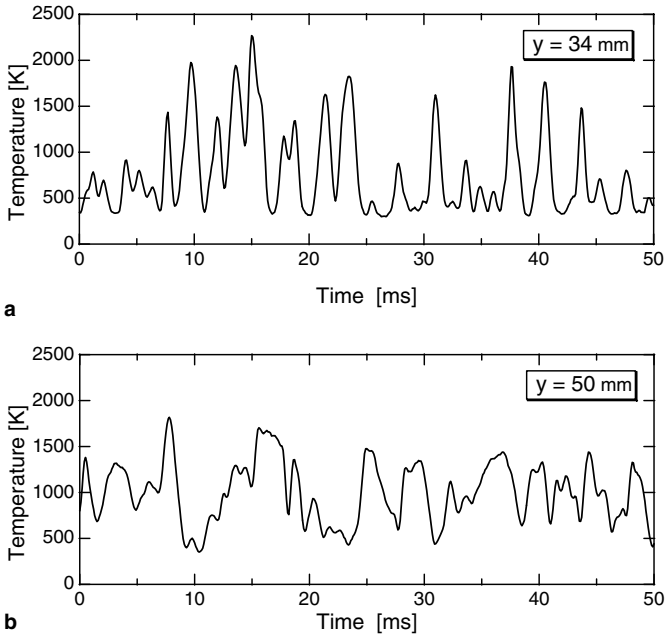

Fig. 7. Signal traces of temperature: (a) $y = 34$ mm and (b) $y = 50$ mm.

counter-gradient heat transfer emerged, there was little correlation between v' and t' ($R_{vt} \simeq 0$), and we could scarcely find the kind of active temperature fluctuation found in the inner-wall region.

The pdf of T at $y = 44$ mm, where the mean-temperature peaked, is not skewed and shows a fairly flat distribution over a wide range of temperature, indicating it to be distinctly different from the pdfs in the inner- and outer-wall regions. This is because low- or high-temperature fluid parcels frequently contact the measurement position of $y = 44$ mm. That position corresponds to the middle of the flame region; therefore, we cannot expect to find unique features compared with those of the inner- and outer-wall regions.

Prior to a further detailed statistical analysis of the combustion field, we examine the influence of the thermocouple time-constant value on the temperature pdf. The change in the pdf distribution at $y = 44$ mm is shown in Fig. 6, in which the time-constant value varied widely (16 ± 4 ms). From Fig. 6, we find that the pdf shape remains similar, though its extent (rms value of temperature fluctuation) is notably changed.[1] In addition, since the correlation coefficient between v' and t', R_{vt}, was scarcely changed even if the time-constant value varied greatly (see Fig. 4), we can neglect the influence of actual uncertainty in the time-constant value in the results of the following statistical analysis.

3.3. Statistical structures of counter-gradient heat transfer

In the above analysis, we have treated velocity and temperature data independently. Since the velocity and temperature of the present combusting flow were measured simultaneously (Tagawa et al., 2002), we can investigate the statistical structures of the turbulent flame from a much closer perspective.

Fig. 8 shows the contours of the joint pdf of v' and t', $P(v', t')$ at the two representative positions mentioned above. The abscissa v' and ordinate t' are normalized by their respective rms values. From the contour of the inner-wall region $y = 34$ mm, we find that the distribution peaks in the fourth quadrant of the (v', t')-plane and extends to the second quadrant with a steep decrease. Since the correlation between v' and t', R_{vt}, at $y = 34$ mm was extremely high, and the rms values v_{rms} and t_{rms} were large (see Fig. 3), the turbulent heat transfer in the inner-wall region is dominated by the well-ordered events of high-temperature ($t' > 0$) fluid parcels approaching the inner wall ($v' < 0$). On the outer-wall side of the flame

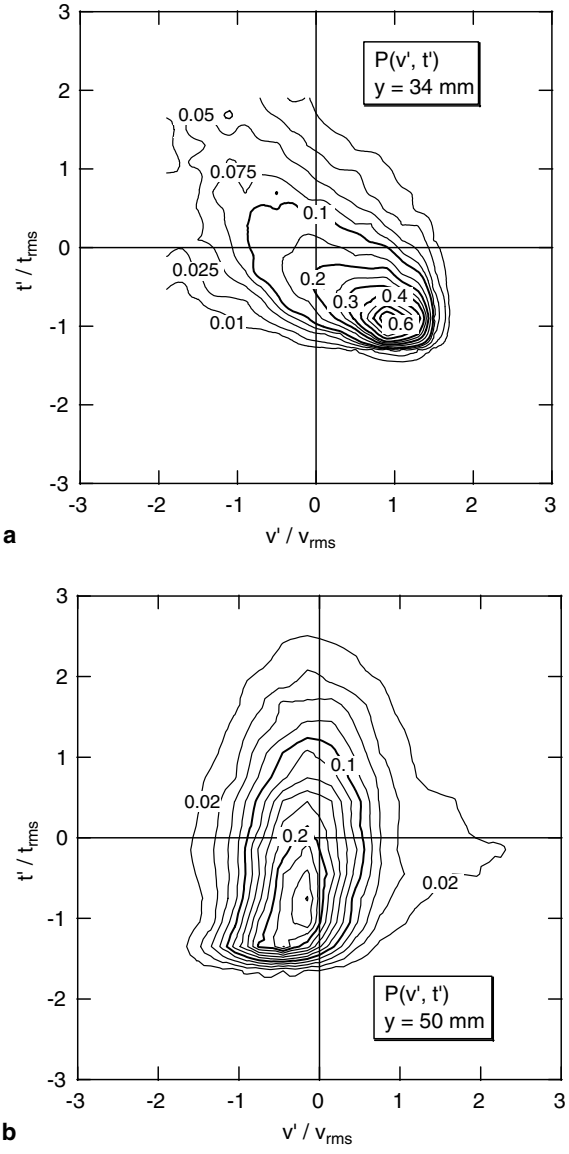

Fig. 8. Joint pdf of v' and t': (a) $y = 34$ mm and (b) $y = 50$ mm.

[1] Since the adiabatic flame temperature of the stoichiometric propane–air mixture is 2261 K (Lewis and von Elbe, 1987), the time-constant value of 20 ms appears to be unlikely.

($y = 50$ mm), the temperature fluctuates mostly independent of v'. As seen in Fig. 5, although the y-direction fluid motions are strongly restrained at $y = 50$ mm, Fig. 8(b) indicates that there exist infrequent but large-amplitude velocity fluctuations ($v' > 0$) having the mean temperature at this position ($t' \simeq 0$).

In order to determine how the above characteristics are reflected in a turbulent heat transfer and to reveal the transport mechanism in detail, we apply a quadrant analysis technique (Lu and Willmarth, 1973) to the present measurements. This technique is a useful tool for analyzing turbulence structures, and has been widely applied to the analysis of various turbulent phenomena, for example, momentum transfer in a boundary layer with premixed combustion (Cheng and Ng, 1985), heat transfer in a non-premixed swirling flame (Hardalupas et al., 1996), heat transfer in a non-premixed jet flame (Caldeira-Pires and Heitor, 2001) and scalar (heat) transfer in wall-bounded turbulent shear flows (Perry and Hoffmann, 1976; Nagano and Tagawa, 1988). In the present study, we classify the turbulent events into the four quadrants in the (v', t')-plane to investigate the turbulence structure of the heat flux $\overline{v't'}$. In the present quadrant decomposition, the events belonging to the four quadrants are termed Q1 ($v' > 0, t' > 0$), Q2 ($v' < 0, t' > 0$), Q3 ($v' < 0, t' < 0$) and Q4 ($v' > 0, t' < 0$).

First, we investigate the fractional contribution of the event Qi to $\overline{v't'}$, $\overline{(v't')}_i$. Fig. 9 shows the results. The sum of the fractional contributions of Qi ($i = 1$–4) equals $\overline{v't'}$. From Fig. 9, we find that, in the inner-wall region, the contributions of Q2 and Q4 are dominant and those of Q1 and Q3 are negligible. The Q2 events—high-temperature fluid motions toward the inner wall—play an especially dominant role in the production of $\overline{v't'}$. In the inner-wall region where the mean-temperature gradient in the y-direction is positive ($\partial\overline{T}/\partial y > 0$), Q2 and Q4 correspond to the gradient diffusion ($v't' < 0$), and Q1 and Q3 to the counter-gradient diffusion ($v't' > 0$). In the outer-wall region, however, since the mean-temperature gradient turns negative, the above correspondence becomes the inverse. That is, Q1 and Q3 correspond to the gradient diffusion, and Q2 and Q4 to the counter-gradient diffusion. As seen in the outer region of Fig. 9, the contributions of Q1 and Q3, which should normally have increased because of the reversal of the sign of the mean-temperature gradient, remain only slightly increased. In particular, the Q1 events—high-temperature ($t' > 0$) fluid motions toward the outer wall ($v' > 0$)—are strongly diminished. The existence of such phenomena was also identified by visual observation of the density field as shown in Fig. 2.

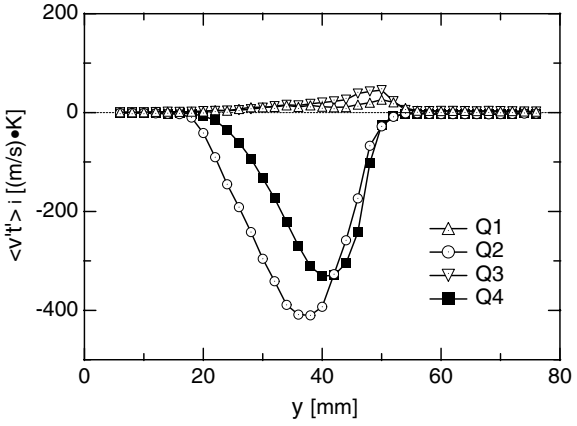

Fig. 9. Fractional contribution to $\overline{v't'}$.

To gain a deeper insight into the relationship between fluid motions and the production of the turbulent heat flux $\overline{v't'}$, we use a weighted pdf analysis technique (Perry and Hoffmann, 1976; Nagano and Tagawa, 1988) (in the following, we call that relationship the internal turbulence structure of $\overline{v't'}$). The weighted pdf of $v't'$, $W_{vt}(v', t')$, is defined by the following equation:

$$W_{vt}(v', t') = v't'P(v', t'). \tag{1}$$

The integration of Eq. (1) within the ith quadrant leads to

$$\overline{(v't')}_i = \int_{Qi} W_{vt}(v', t')\,\mathrm{d}v'\,\mathrm{d}t'. \tag{2}$$

Since Eq. (2) gives the fractional contribution $\overline{(v't')}_i$ shown in Fig. 9, we can investigate in detail the internal structure of $\overline{v't'}$ using the weighted pdf given by Eq. (1).

Fig. 10 shows the results. From the contour at $y = 34$ mm (the upper figure), the internal structures of Q2 and Q4 are seen to be totally different, although both events are the elements of the gradient-diffusion phenomena. Specifically, the weighted pdf of Q2—high-temperature fluid motion toward the inner wall—shows a low and broad distribution, while that of Q4—low-temperature fluid motion toward the outer wall—has a high and narrow distribution. In the outer-wall region ($y = 50$ mm) where the counter-gradient heat transfer emerged, the high-temperature ($t' > 0$) fluid motion toward the outer wall ($v' > 0$)—the Q1 event and the gradient diffusion phenomenon in this region—is, in particular, strongly restrained. The results of Fig. 10 show that the onset of a counter-gradient heat transfer is caused principally by the existence of such phenomena. In short, the internal structure of $\overline{v't'}$ indicates that the motion of the low-density fluid approaching the outer wall (the high-pressure side) tends to be preferentially damped or to be occasionally forced back to the inner-wall side because of the r-direction pressure gradient externally imposed on the flow field.

3.4. Spatio-temporal structure of thermal field

To reveal the turbulent structure of the above two contrasting thermal fields, we measured the spatio-temporal correlation coefficient R, which is defined as the two-point correlation for a fluctuating temperature field:

$$R(\theta_0, y_0;\ \theta, y;\ \Delta\tau) = \frac{\overline{t'(\theta_0, y_0, \tau)\cdot t'(\theta, y, \tau + \Delta\tau)}}{t_{\mathrm{rms}}(\theta_0, y_0)\cdot t_{\mathrm{rms}}(\theta, y)}, \tag{3}$$

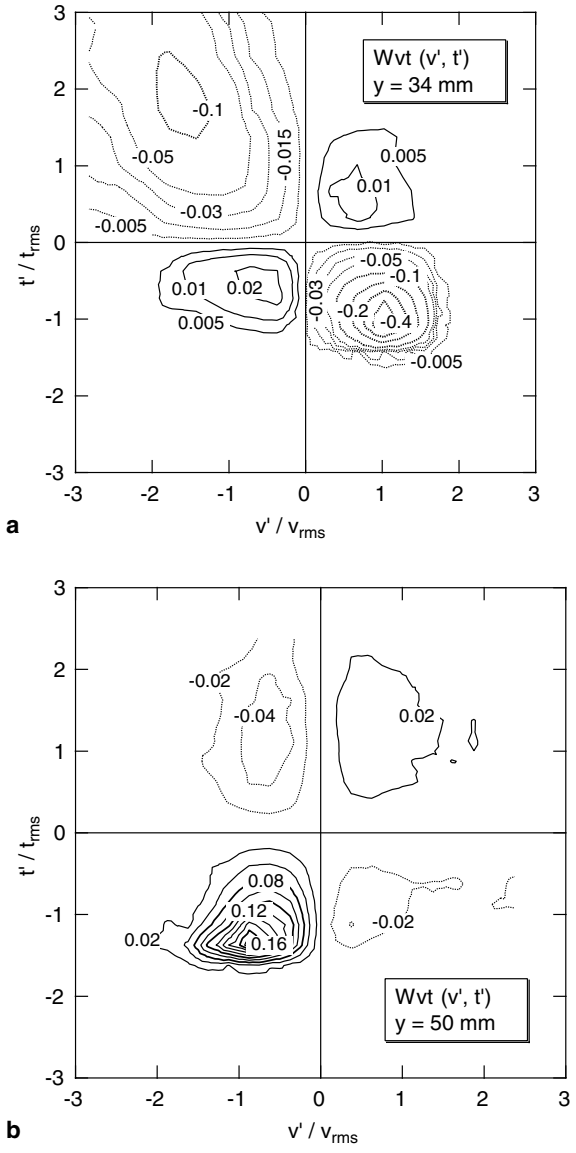

Fig. 10. Weighted pdf of $v't'$: (a) $y = 34$ mm and (b) $y = 50$ mm.

where $t'(\theta_0, y_0, \tau)$ and $t'(\theta, y, \tau + \Delta\tau)$ denote temperature fluctuation at a time τ and a reference (fixed) point (θ_0, y_0) and at $\tau + \Delta\tau$ and an arbitrary point (θ, y), respectively. In this experiment, we measured the correlation R over a test section of $(45°, 0\text{ mm}) \leqslant (\theta, y) \leqslant (75°, 80\text{ mm})$ in the central $(z = 0\text{ mm})$ plane. In the measurement, two fine-wire thermocouple probes were used to obtain a two-dimensional distribution of R, one fixed at a reference point (θ_0, y_0) and the other moved so as to scan the test section downstream of the reference point. Two y_0 positions on the $\theta_0 = 45°$ line were selected as the reference points so that $\overline{T}$ took the mean of its minimum $\overline{T}_{\min}$ and its maximum $\overline{T}_{\max}$, that is, $(\overline{T}_{\min} + \overline{T}_{\max})/2 \simeq 1100$ K. Specifically, these two points were $(\theta_0, y_0) = (45°, 36\text{ mm})$ and $(45°, 48\text{ mm})$.

Fig. 11 shows the contour maps of R for which the reference probe was fixed at the inner-wall side of the flame $(45°, 36\text{ mm})$. As shown in Fig. 11, the positive correlation region expanding slightly to the inner-wall side [Fig. 11(a);

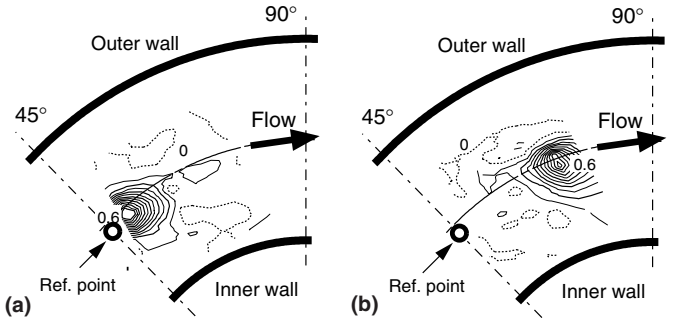

Fig. 11. Spatial structure of the inner thermal field: $(\theta_0, y_0) = (45°, 36\text{ mm})$: (a) $\Delta\tau = 1$ ms and (b) $\Delta\tau = 5$ ms.

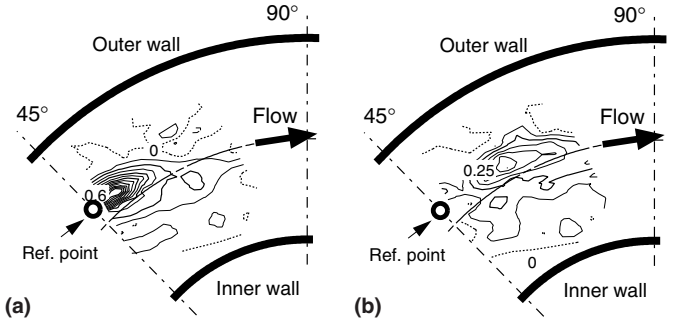

Fig. 12. Spatial structure of the outer thermal field: $(\theta_0, y_0) = (45°, 48\text{ mm})$: (a) $\Delta\tau = 1$ ms and (b) $\Delta\tau = 5$ ms.

$\Delta\tau = 1$ ms] is advected with little diffusion along the duct centerline, and remains relatively large in scale [Fig. 11(b); $\Delta\tau = 5$ ms], while part of it is outside of the test section. Fig. 12, on the other hand, shows the contour maps of R for which the reference point was located on the outer-wall side $(45°, 48\text{ mm})$. The positive correlation region in the outer thermal field [Fig. 12(a)] starts to move downstream in a way similar to that indicated in Fig. 11. However, at $\Delta\tau = 5$ ms [Fig. 12(b)], the region shrinks in the r-direction with its peak value decreasing rapidly. Hence, the correlation region appears to be stagnated and dissipated in the vicinity of the reference point.

The temporal variations of R shown in Figs. 11 and 12 represent the processes of advection and dissipation of the spatial temperature patterns formed by turbulent mixing of high-temperature fluid parcels (mainly burnt gas) and low-temperature ones (mainly air). Thus, the onset mechanism of the strong gradient-type diffusion heat transfer on the inner-wall side of the flame and that of the weak counter-gradient one on the outer-wall side are clearly reflected in the characteristics of the spatio-temporal structures of the thermal fields shown in Figs. 11 and 12. On the inner-wall side where the strong gradient-type diffusion heat transfer occurs, spatial temperature patterns generated by turbulent mixing of hot and cold gas parcels can grow downstream with little diffusion. However, the temperature patterns on the outer-wall side of the flame are attenuated rapidly and diffused into a background fluctuating temperature field. As a result, as seen from Fig. 12, the positive

correlation region is scarcely advected downstream and dissipates in the vicinity of the reference point.

4. Conclusions

The structure of the thermal field of a non-premixed turbulent flame formed in a curved-rectangular duct was investigated experimentally. The results showed the onset of the counter-gradient diffusion heat transfer—an anomalous phenomenon in turbulent transport processes—on the outer-wall side of the flame and, in contrast, a strong gradient-diffusion on the inner-wall side. The characteristics of the turbulent heat transfer were strongly affected by the pressure gradient in the radial direction of the curved duct.

To identify the onset mechanism of the counter-gradient diffusion in heat transfer, we investigated the statistical characteristics of a combustion field using the quadrant analysis technique and the two-point correlation measurement technique—useful tools for analyzing the structure of turbulent phenomena. As a result, in the outer-wall region of the flame, the motion of high-temperature fluid parcels was preferentially damped, leading to the onset of a weak counter-gradient diffusion. The spatio-temporal correlation structure of the thermal field can be well explained by the onset mechanism of the counter-gradient diffusion of the thermally stratified turbulent flows so far reported (Komori and Nagata, 1996).

The turbulence characteristics of the present combustion field should be a function of the pressure gradient in the radial direction (i.e., the duct curvature and/or the mean velocity at the combustor inlet), the radial position of the fuel exit, the rate of heat release, etc. However, there is not sufficient information for revealing the function at present. Thus, we need further detailed studies on the transport characteristics of the turbulent combustion field formed in a curved-duct flow.

Acknowledgements

The authors are indebted to Dr. H. Morikita, Professors K. Hishida and M. Maeda at Keio University for their expertise and advice on the LDV measurement. This research is partially supported by Grants-in-Aid for Scientific Research from the Japan Society for the Promotion of Science (Grant Nos. 17106003 and 12650202).

Appendix A. Bias error in the LDV measurement

The LDV measurements may suffer from bias errors due to a kind of conditional sampling—the LDV measurements can be weighted toward the data of high velocity and/or of dense particle seeding (Durst et al., 1976). Since the seeding particles were distributed very sparsely in the present experiment, the data rate (detection frequency) of the Doppler signals was quite low—ranging from 10 to 50 times per second. Thus, the present measurements can be considered to be free from bias errors. Nevertheless, in the appendix, we did review the bias errors in the present measurements to confirm that they are actually negligible.

First, we modeled a combustion field as shown in Fig. A.1 in order to reveal the nature of the bias errors. It is noted that a similar model was used to explain the counter-gradient diffusion of a premixed turbulent flame (Libby and Bray, 1981), though the purpose was different from the present one. The thick solid lines in Fig. A.1 show V, T and ρ (gas density) from the top. We assumed that the gas density ρ fluctuates between ρ_0 (low-temperature region) and $\gamma\rho_0$ (high-temperature region) with $0 < \gamma \leqslant 1$, and the seeding particle number density is in direct proportion to ρ. Then, the detection frequency of the Doppler signals is also directly proportional to ρ. The temperature data sampled in synchronization with the LDV measurements are indicated by the open circle in Fig. A.1. As a result, the simultaneous measurements of V and T are to be weighted toward those of high gas-density regions.

From Fig. A.1, the mean temperature obtained from the simultaneous measurements, $\overline{T}_R$, is given by

$$\overline{T}_R = (\overline{T} - t_{\mathrm{rms}})\left(1 - \frac{\gamma}{2}\right) + (\overline{T} + t_{\mathrm{rms}})\frac{\gamma}{2} = \overline{T} - (1-\gamma)t_{\mathrm{rms}}, \tag{A.1}$$

where $\overline{T}$ denotes a true mean temperature. From Eq. (A.1), the temperature fluctuation of the simultaneous measurement is written as

$$\left.\begin{aligned} t'_{\mathrm{H}} &= (\overline{T} + t_{\mathrm{rms}}) - \overline{T}_R = (2-\gamma)t_{\mathrm{rms}}, \\ t'_{\mathrm{L}} &= (\overline{T} - t_{\mathrm{rms}}) - \overline{T}_R = -\gamma t_{\mathrm{rms}}, \end{aligned}\right\} \tag{A.2}$$

where the subscript H denotes the value in the high-temperature region, and L in the low-temperature region. From Eqs. (A.1) and (A.2), we can calculate the second- and third-order moments of temperature fluctuation, $(\overline{t'^2})_R$ and $(\overline{t'^3})_R$, which are simultaneous measurements of the temperature field. The temperature skewness, $S_R(t)$, can

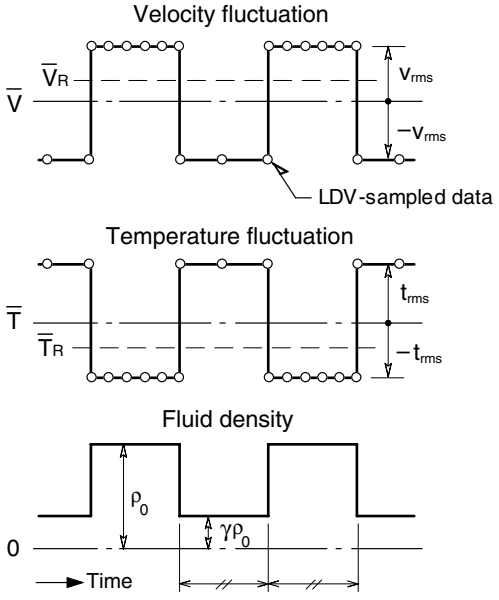

Fig. A.1. Modeled signal traces sampled by LDV.

also be derived from the moments. The results are as follows:

$$\left.\begin{aligned}(\overline{t'^2})_R &= (t'_{\mathrm{L}})^2\left(1-\tfrac{\gamma}{2}\right)+(t'_{\mathrm{H}})^2\tfrac{\gamma}{2}\\ &= \gamma(2-\gamma)t^2_{\mathrm{rms}},\\ (\overline{t'^3})_R &= (t'_{\mathrm{L}})^3\left(1-\tfrac{\gamma}{2}\right)+(t'_{\mathrm{H}})^3\tfrac{\gamma}{2}\\ &= 2\gamma(2-\gamma)(1-\gamma)t^3_{\mathrm{rms}},\\ S_R(t) &= \frac{(\overline{t'^3})_R}{(\overline{t'^2})_R^{3/2}} = \frac{2(1-\gamma)}{\sqrt{\gamma(2-\gamma)}}.\end{aligned}\right\} \tag{A.3}$$

Using Eq. (A.3), we can numerically evaluate the bias errors of the temperature statistics. For example, when $\gamma = 1/4$, we obtain $\sqrt{(\overline{t'^2})_R} = 0.66 t_{\mathrm{rms}}$ and $S_R(t) = 2.27$. The true values of these quantities should be t_{rms} and 0, respectively. Hence, if the measurement model shown in Fig. A.1 is appropriate, significant bias errors will be introduced into these temperature statistics.

On the basis of the above consideration, we can quantitatively appraise the bias errors in the present experiment by comparing the present simultaneous measurement data with the continuously sampled thermocouple measurements that are free from the above bias errors. Fig. A.2 shows the comparison of the t_{rms} and $S(t)$ values between these two measurement techniques. As seen from Fig. A.2, we can barely find any statistical differences between the simultaneous and continuous measurements over almost the entire region of the flame. This indicates that the present simultaneous measurements are almost free from bias errors. At both ends of the flame region ($y \leqslant 18$ mm and $y \geqslant 54$ mm), where the temperature signals scarcely appear, there is a quantitative difference in $S(t)$ between the two techniques. However, this is not due to bias errors but because the electric noise of the temperature signals simultaneously measured with LDV was 2–3 times as high as that of the original thermocouple signals continuously measured (this is because the additional noise originating from the laser light source of the LDV can seep into the simultaneous measurements). As shown in Fig. A.2, a high-order turbulence quantity such as the skewness factor is also free from bias errors, and thus we conclude that the bias errors due to the above conditional sampling did not affect the simultaneous measurement data.

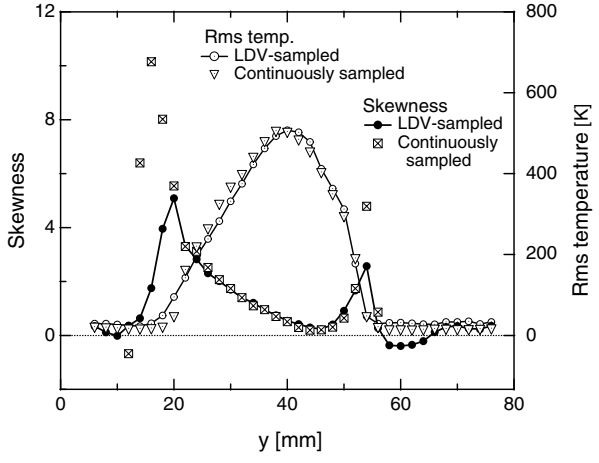

Fig. A.2. LDV-sampling effects on temperature statistics.

References

Bray, K.N.C., 1995. Turbulent transport in flames. Proc. R. Soc. Lond. A 451, 231–256.

Caldeira-Pires, A., Heitor, M.V., 2001. Characteristics of turbulent heat transport in nonpremixed jet flames. Combust. Flame 124, 213–224.

Cheng, R.K., Ng, T.T., 1985. Conditional Reynolds stress in a strongly heated turbulent boundary layer with premixed combustion. Phys. Fluids 28, 473–488.

Durst, F., Melling, A., Whitelaw, J.H., 1976. Principles and Practice of Laser-Doppler Anemometry. Academic Press, London, p. 197.

Hardalupas, Y., Tagawa, M., Taylor, A.M.K.P., 1996. Characteristics of counter-gradient heat transfer in a non-premixed swirling flame. In: Adrian, R.J. et al. (Eds.), Developments in Laser Techniques and Applications to Fluid Mechanics. Springer-Verlag, Berlin, pp. 159–184.

Jones, W.P., 1994. Turbulence modelling and numerical solution methods for variable density and combusting flows. In: Libby, P.A., Williams, F.A. (Eds.), Turbulent Reacting Flows. Academic Press, London, pp. 309–374.

Kalt, P.A.M., Chen, Y.-C., Bilger, R.W., 2002. Experimental investigation of turbulent scalar flux in premixed stagnation-type flames. Combust. Flame 129, 401–415.

Komori, S., Nagata, K., 1996. Effects of molecular diffusivities on counter-gradient scalar and momentum transfer in strongly stable stratification. J. Fluid Mech. 326, 205–237.

Lewis, B., von Elbe, G., 1987. Combustion, Flames and Explosions of Gases. Academic Press, Orlando, p. 720.

Libby, P.A., Bray, K.N.C., 1981. Countergradient diffusion in premixed turbulent flames. AIAA J. 19, 205–213.

Lu, S.S., Willmarth, W.W., 1973. Measurements of the structure of the Reynolds stress in a turbulent boundary layer. J. Fluid Mech. 60, 481–511.

Luo, K.H., Bray, K.N.C., 1998. Combustion-induced pressure effects in supersonic diffusion flames. Proc. Combust. Inst. 27, 2165–2171.

Nagano, Y., Tagawa, M., 1988. Statistical characteristics of wall turbulence with a passive scalar. J. Fluid Mech. 196, 157–185.

Nishiki, S., Hasegawa, T., Borghi, R., Himeno, R., 2002. Analyzing and modeling of transport properties of turbulent kinetic energy and turbulent scalar flux in turbulent premixed flames by DNS. J. Combust. Soc. Jpn. 44, 47–57 (in Japanese).

Perry, A.E., Hoffmann, P.H., 1976. An experimental study of turbulent convective heat transfer from a flat plate. J. Fluid Mech. 77, 355–368.

Rutland, C.J., Cant, R.S., 1994. Turbulent transport in premixed flames. In: Proc. Summer Program, Center for Turbulence Research, NASA Ames/Stanford Univ., pp. 75–94.

Tagawa, M., Ohta, Y., 1997. Two-thermocouple probe for fluctuating temperature measurement in combustion—rational estimation of mean and fluctuating time constants. Combust. Flame 109, 549–560.

Tagawa, M., Nagaya, S., Ohta, Y., 2001. Simultaneous measurement of velocity and temperature in high-temperature turbulent flows: a combination of LDV and a three-wire temperature probe. Exp. Fluids 30, 143–152.

Tagawa, M., Matsubara, F., Ohta, Y., 2002. Heat transfer characteristics of a non-premixed turbulent flame formed in a curved rectangular duct. Combust. Flame 129, 151–163.

Veynante, D., Poinsot, T., 1997. Effects of pressure gradients on turbulent premixed flames. J. Fluid Mech. 353, 83–114.

Veynante, D., Trouvé, A., Bray, K.N.C., Mantel, T., 1997. Gradient and counter-gradient scalar transport in turbulent premixed flames. J. Fluid Mech. 332, 263–293.

Zhang, S., Rutland, C.J., 1995. Premixed flame effects on turbulence and pressure-related terms. Combust. Flame 102, 447–461.